Supporting Information for

"Self-propelling nanomotors in the presence of strong Brownian forces"

Tung-Chun Lee, Mariana Alarcón-Correa, Cornelia Miksch, Kersten Hahn, John G. Gibbs, Peer Fischer*

*e-mail: fischer@is.mpg.de

Table of contents

S1. Experimental procedures

Materials

Poly(styrene)-b-poly(2-vinylpyridine) (S units: 1056; VP units: 671) diblock copolymer was supplied by Polymer Source, Canada. Silicon (100) wafers were supplied by CrysTec GmbH, Germany. Chemicals were used as received unless otherwise specified. Hydrogen hexachloroplatinate(IV) hexahydrate ($H_2PtCl_6 \cdot 6H_2O$) and sodium citrate tribasic dehydrate 99% were supplied by Sigma-Aldrich and Fluka, respectively. All solvents are analytical grade and were used as received unless otherwise stated. Deionized water with 18.2 MΩ resistivity was used (Milli-Q ultrapure system). Hydrogen peroxide 31% was obtained from BASF. For the fabrication of Au-Au NPs polystyrene(1056)-*block*-poly(2-vinylpyridine)(671) and $HAuCl_4 \bullet 3H_2O$ powder were used, supplied by the same sources as in the Pt case.

General instruments

TePla PS210 microwave plasma system was used for W10 (10% H_2, 90% Ar) plasma treatment, while PVA TePla PS100 microwave plasma system was used for oxygen plasma treatment. An Eppendorf MiniSpin plus centrifuge was used.

Preparation of the Pt NP arrays

The hexagonal array of platinum nanoparticles (Pt NPs) was prepared using block copolymer micellar nanolithography (BCML) as previously reported.[1] Briefly, poly(styrene)-b-poly(2-vinylpyridine) (S units: 1056; VP units: 671) was dissolved in toluene at a concentration of 4 mg/mL and stirred overnight. To the polymer solution, $H_2PtCl_6 \cdot 6H_2O$ powder was added at a molar ratio of 0.4 per vinylpyridine unit and stirred at least 72 hours to yield self-assembled micelles loaded with H_2PtCl_6 in the cores. The micelles were then transferred as a uniform monolayer onto the piranha cleaned silicon wafer by spin coating techniques. After that, the wafer was treated under W10 plasma (350W, 0.4mbar) for 45 min. In this step, the polymer shell was removed and H_2PtCl_6 was reduced, forming a regular quasi-hexagonal array of 10 nm Au NPs separated by 62± 8nm (as measured by SEM with an in-lens detector).

Deposition of gold by glancing angle deposition (GLAD)

The deposition of the gold on the platinum seeds was performed in a vacuum chamber with pressures in the range 10^{-7}- 10^{-6} torr, by electron-beam evaporation. The substrate was tilted at 85 degree with respect to the flux and was constantly rotating. No substrate cooling was used. Same procedure was followed for the deposition of the control Au-Au NP samples and for the 60-nm Pt-Pt-Au JNPs. For the latter, a layer of Pt was first deposited to increase the Pt seed size, followed by a deposition of Au. A Ti layer between

the Pt and the Au was used to increase the adherence. The angle of deposition and rotation speed was kept constant during all depositions.

Preparation of nanocolloidal solution

Pt-Au Janus nanoparticles (JNPs) and Au-Au nanoparticles (NPs) were lifted off from the wafer by sonicating a piece of sample wafer (~1 cm^2) in an aqueous solution of 1 mM sodium citrate for ~15 min, resulting in a nanocolloidal solution of JNPs / NPs. The JNPs / NPs could be concentrated by centrifugation (12100 g, 60 min) and redispersed in a desired amount of solvent.

Transmission electron microscopy (TEM)

TEM samples were prepared by drop casting ~10 µL of the nanocolloidal solution onto a Holey® carbon coated TEM grid (Cu 400 mesh), followed by drying. The sample loaded TEM grid was then washed (deionized water) to remove excess salts, and finally dried. Bright field TEM images were recorded on a Philips CM200 under an accelerating voltage of 200 kV.

Scanning transmission electron microscopy (STEM)

STEM was conducted using Zeiss SESAM under an accelerating voltage of 200 kV. High-angle annular dark field STEM (HAADF-STEM) images and STEM energy dispersive X-ray (STEM-edx) elemental maps were recorded with a 20-µm top-hat objective aperture and at a tilt angle of 20° to maximize the X-ray signal.

Dynamic light scattering (DLS)

Dynamic light scattering measurements were conducted using a Malvern Zetasizer Nano Z with 40-µL disposable micro cuvettes. Nanocolloidal solutions of Pt-Au JNPs and Au-Au NPs in the presence of 1 mM sodium citrate were filtered with a syringe filter (Whatman FP 30/0.2, pore size 0.2µm). The appropriate amount of H_2O_2 was added and the solution was sonicated prior to the DLS experiments. For samples with higher H_2O_2 concentrations, sonication was conducted in-between measurements whenever necessary to remove gas bubbles formed on the cuvette wall. Measurements were carried out on the same day of the preparation of the nanocolloidal solution. The instrument scattering angle is 173° and the sample temperature was 25°C. The general purpose analysis model from Malvern Zetaseizer software 7.02 was used.

Dark field optical microscopy

Dark field microscopy videos were taken on a Zeiss AxioObserver.Z1 inverted microscope with an attached Basler acA2000-340kc camera. Videos were taken at a frame rate of 12 frames per second. A nanocolloidal solution of 60-nm Pt-Pt-Au JNPs, in presence of 1 mM aqueous sodium citrate was filtered with a syringe filter (Whatman FP 30/0.2, pore size 0.2 µm) prior to dark field optical microscopy imaging. 25 µL of 60-nm Pt-Pt-Au Janus particles suspended in glycerol/citrate/H_2O (+H_2O_2) were added by pipette onto a cleaned glass slide. Glycerol was added to both samples in order to increase the viscosity, effectively slowing the particles, and facilitating easy tracking. A square, double-sided piece of tape with the center removed created a well (~25 μL) into which the fluid was placed, then a clean glass cover slip was adhered to the top of the tape closing off the sample from its surroundings. A 100x objective (NA = 1.25, oil immersion) coupled with a dark filed condenser (NA = 1.2/1.4) collected light scattered from the Janus nanoparticles. Particle tracking was performed using the ImageJ plugin MTrack2, but due to the low contrast of the video data, significant particle-linking and manual tracking, also in ImageJ, had to be applied as well.

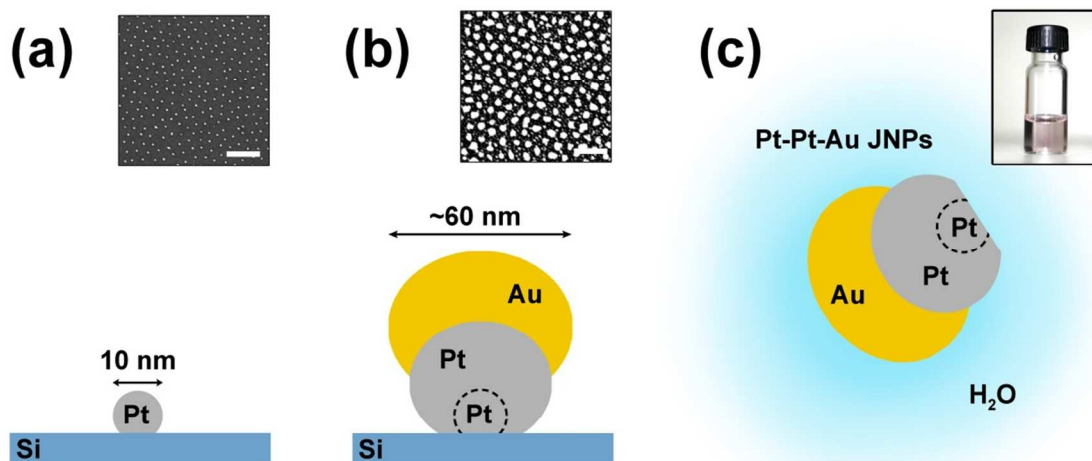**S2. Fabrication scheme for the 60-nm Pt-Pt-Au JNPs**

Figure S1. Fabrication scheme of 60-nm Pt-Pt-Au JNPs. (a) A hexagonal array of Pt-nanoseeds was generated by block copolymer micelle lithography on silicon wafer. Inset: Scanning electron micrograph (SEM) of the resultant nano-patterned surface. Scale bar = 200 nm. (b) Elemental platinum, followed by gold were sequentially deposited onto the Pt-nanoseeds by glancing angle deposition (GLAD) producing an array of Pt-Pt-Au Janus nanoparticles. Inset: SEM of the resultant Pt-Pt-Au JNPs. Scale bar = 200 nm. (c) Pt-Pt-Au JNPs can be lifted off easily by sonication to yield a stable aqueous nanocolloidal solution. Inset: Photograph showing Pt-Pt-Au JNPs nanocolloidal solution.

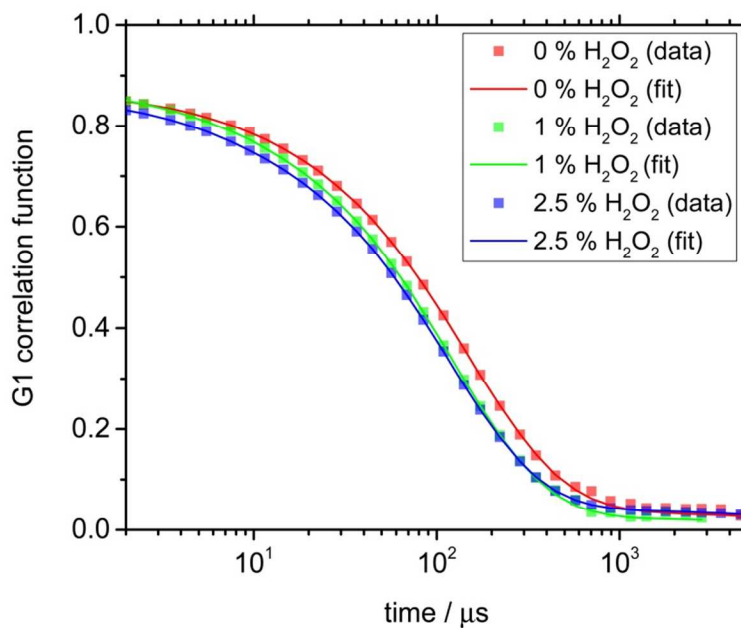## S3. Additional data on dynamic light scattering measurements

Figure S2. Correlograms and G1 correlation fits of 30-nm Pt-Au JNPs in respectively 0 %, 1 % and 2.5 % H_2O_2.
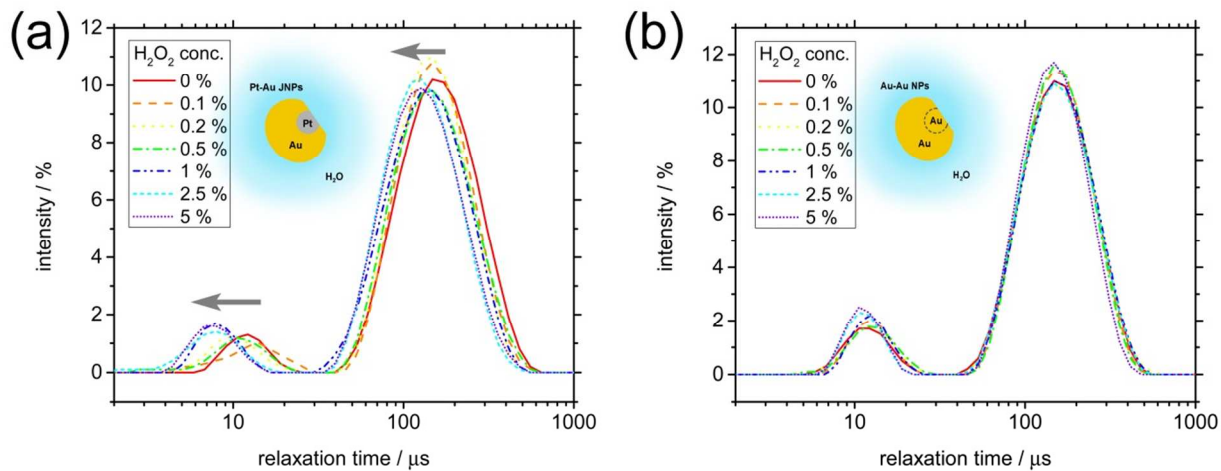

Figure S3. Translational and rotational relaxation plot of (a) 30-nm Pt-Au JNPs and (b) Au-Au NPs for increasing H_2O_2 concentrations. Significant shift in the relaxation peaks is observed (marked by grey arrows) only in the case of catalytically active Pt-Au JNPs.

S4. Apparent hydrodynamic size

Table S1. Apparent hydrodynamic size in nm based on translational and rotational relaxation of the 30-nm Pt-Au JNPs and Au-Au NPs under various H_2O_2 concentrations. Data based on scattering intensity and scattering volume is shown for comparison, where the former is more significantly affected by the signal of dimers. The data scaled based on volume shows a much better match with the TEM size of a single NP (33.3±3.6 nm x 28.8±3.2 nm). While showing the same overall trend, data based on volume is more sensitive to random errors from the measurement and is therefore not considered in the analysis of the manuscript.

			H_2O_2 concentration / %						
			0	0.1	0.2	0.5	1	2.5	5
intensity	Pt-Au JNPs	translation	53.4	51.9	50.0	49.9	45.3	43.2	43.4
		rotation	48.3	50.0	45.6	45.1	42.7	40.5	41.8
	Au-Au NPs	translation	52.5	53.4	53.1	53.5	53.8	52.7	51.2
		rotation	49.2	50.0	50.2	50.5	50.2	48.5	48.5
volume	Pt-Au JNPs	translation	29.7	34.1	29.9	27.5	29.9	—*	23.4
		rotation	51.2	50.7	48.3	44.5	47.6	39.8	44.0
	Au-Au NPs	translation	34.6	34.6	34.6	34.6	34.6	31.9	31.9
		rotation	45.8	47.2	46.7	45.6	47.6	46.3	46.2

* Signal too weak to be extracted after scaling.

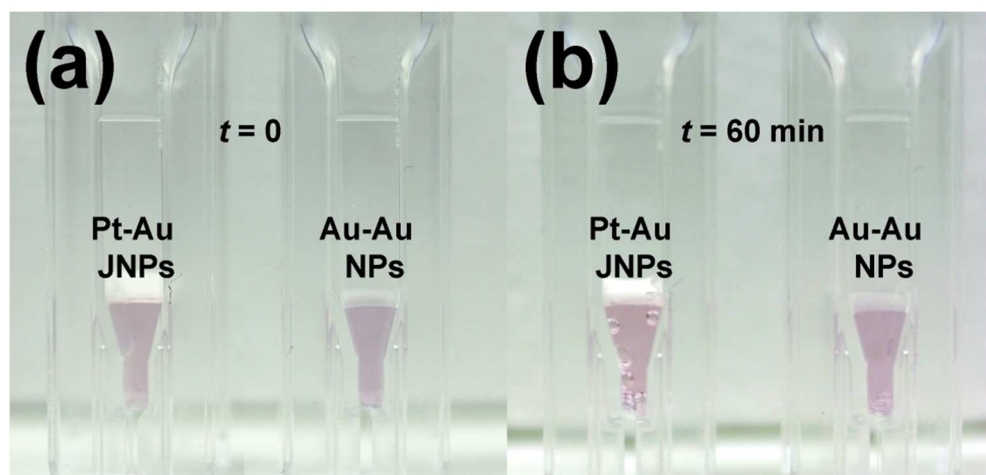## S5. Formation of macroscopic bubbles from Pt-Au JNP catalysis

Figure S4. Nanocolloidal solutions of 30-nm Pt-Au JNPs and Au-Au NPs (a) immediately and (b) 60 min after the addition of H_2O_2 (final concentration = 1% *v/v*). After 60 min, the formation of macroscopic gas bubbles is observed only in the case of Pt-Au JNPs, verifying the catalytic activity of the Pt in the JNPs towards the disproportionation of H_2O_2. The Au-Au NPs are catalytically inactive, as expected.

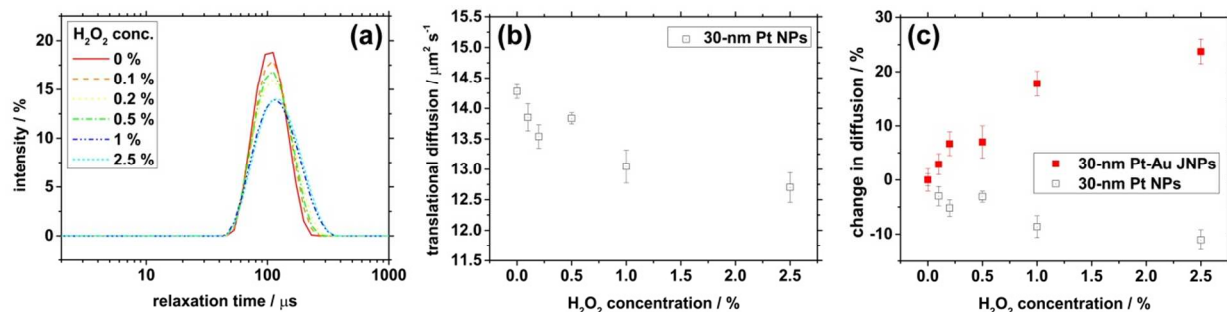**S6. Control experiments using 30-nm Pt NPs and Pt-Pt NPs**

Figure S5. (a) Translational relaxation plot of commercial 30-nm Pt NPs (nanoComposix: NanoXact, citrate stabilized) as a function of increasing H_2O_2 concentrations. No significant shift in the relaxation peaks is observed. (b) Translational diffusion constant of 30-nm Pt NPs for different concentrations of H_2O_2. The slight decrease in diffusion constant could be due to the minor increase in viscosity upon addition of H_2O_2. (c) Percentage change of translational diffusion constants as a function of the H_2O_2 concentration. All measurements were conducted with the same sample concentration as that for the 30-nm Pt-Au JNPs ($\sim 3 \times 10^{10}$ NPs/mL).
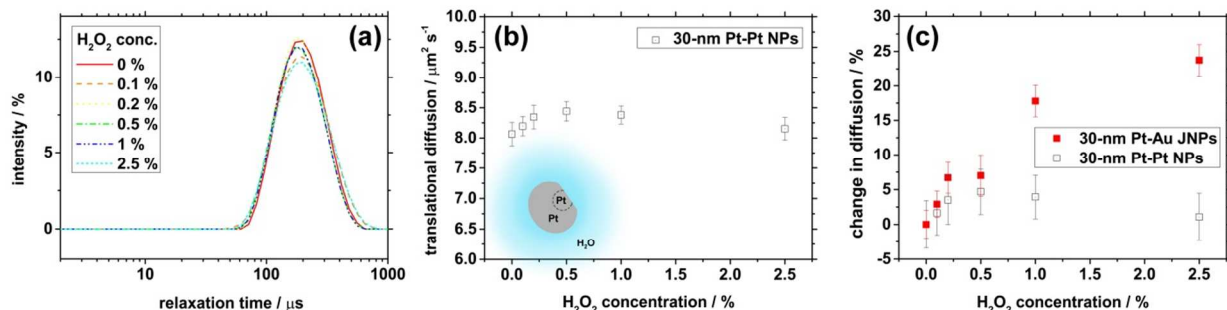

Figure S6. (a) Translational relaxation plot of 30-nm Pt-Pt NPs made by our GLAD system as a function of increasing H_2O_2 concentrations. No significant shift in the relaxation peaks is observed. (b) Translational diffusion constant of 30-nm Pt-Pt NPs for different concentrations of H_2O_2. Inset showing a schematic diagram of a Pt-Pt NP. (c) Percentage change of translational diffusion constants as a function of the H_2O_2 concentration. All measurements were conducted with the same sample concentration as that for the 30-nm Pt-Au JNPs ($\sim 3 \times 10^{10}$ NPs/mL).

9

S7. Control experiments using 100-nm inactive particles mixed with active JNPs
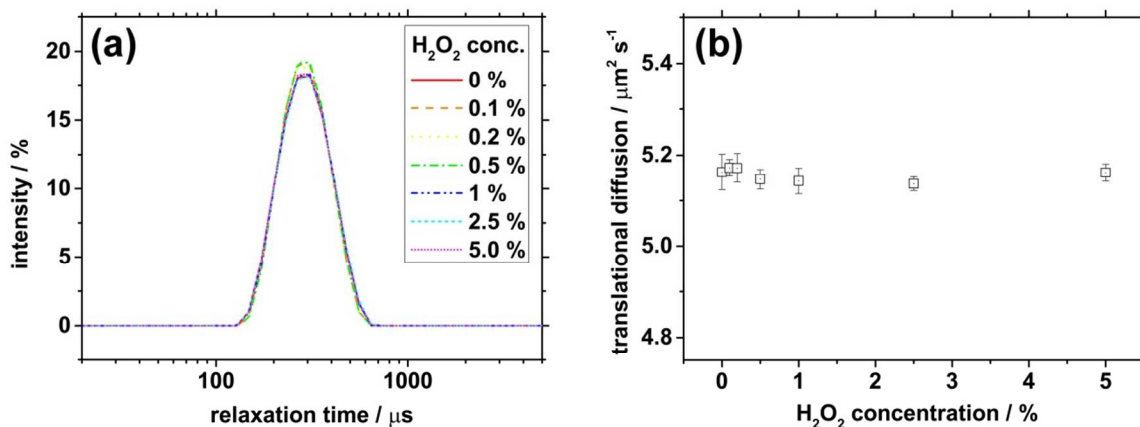

Figure S7. (a) Translational relaxation plot of a mixture of 30-nm Pt-Au JNPs and 100-nm polystyrene particles (Latex beads, polystyrene, supplied by Sigma-Aldrich) for increasing H_2O_2 concentrations. Since the scattering intensity scales with r^6, where r is the radius of the scattering particles, the signal of 100-nm polystyrene particles dominates the DLS signal, even though the number ratio of 30-nm Pt-Au JNPs to 100-nm polystyrene particles is ~20:1. No significant shift in the relaxation peaks is observed. (b) Apparent translational diffusion constant of 100-nm polystyrene particles (in the presence of 30-nm Pt-Au JNPs) for different concentrations of H_2O_2. This data is extracted by considering that the convoluted relaxation peak corresponds to a single type of scatterer. This is a conservative assumption because there is a minor contribution from the active Pt-Au JNPs that would increase the apparent translational diffusion in accord with the different H_2O_2 concentrations.

It is challenging to distinguish the rotational and translational diffusion of the 30-nm Pt-Au JNPs, plus the translational diffusion of the 100-nm PS particles. Hence, we have chosen the number ratio of the 30-nm Pt-Au JNPs to the 100-nm PS particles to be ~20:1, such that the signal of the 100-nm PS particles dominates. At the same time, we try to keep the Pt-Au JNPs in excess with respect to the PS particles, to avoid "false positive" data. It is noted that false positive data could be generated when the enhanced diffusion of the inactive PS particles is induced by direct bombardment of the active Pt-Au JNPs (even in the absence of nanobubbles). This effect has been reported in similar systems at the microscale.[2, 3] However, for large excess of the active swimmers, the enhanced diffusion of the inactive particles will reduce, since the random bombardments from the active swimmers become so frequent that they will effectively cancel each other.
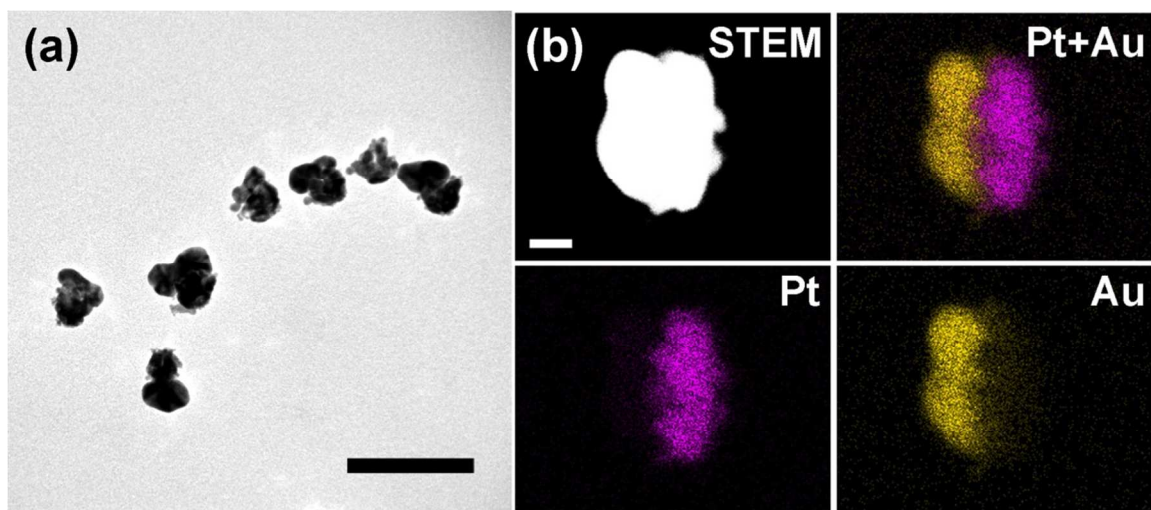
S8. TEM images of 60-nm Pt-Pt-Au JNPs and Au-Au NPs

Figure S8. (a) Transmission electron micrograph of 60-nm Pt-Pt-Au JNPs. (b) High-angle annular dark field (HAADF) STEM image and STEM-edx elemental maps of a selected Pt-Pt-Au JNP. Scale bars = (a) 100 nm; (b) 20 nm.
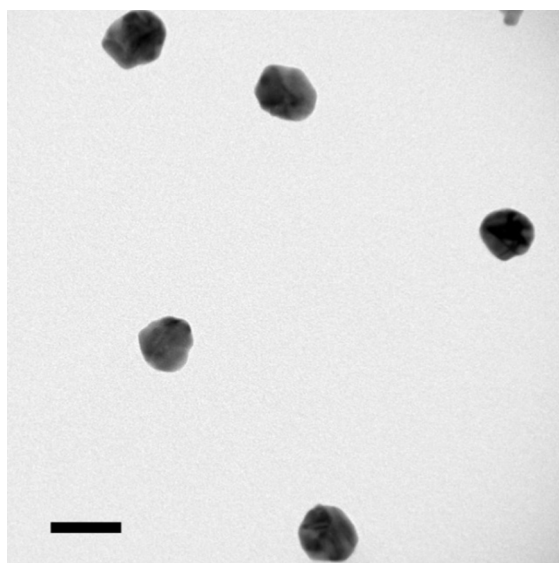

Figure S9. TEM image of Au-Au NPs. Scale bar = 50 nm.

S9. Dark field optical microscopy movies

Movie S1. Dark field microscopy video (10 s) of diffusion (Brownian motion) of the 60-nm Pt-Pt-Au Janus nanoparticles in 50% glycerol. Videos were taken at 12 fps with an oil immersion 100X objective (NA = 1.25). Scale bar = 1 μm.

Movie S2. Dark field microscopy video (10 s) was taken under the same conditions as Movie S1, but with 1.5% H_2O_2 increasing the overall effective diffusion of the JNPs. Scale bar = 1 μm.

References

1. Glass, R.; Möller, M.; Spatz, J. P. *Nanotechnology* **2003,** 14, 1153.
2. Mino, G.; Mallouk, T. E.; Darnige, T.; Hoyos, M.; Dauchet, J.; Dunstan, J.; Soto, R.; Wang, Y.; Rousselet, A.; Clement, E. *Phys. Rev. Lett.* **2011,** 106, 048102.
3. Wilson, L. G.; Martinez, V. A.; Schwarz-Linek, J.; Tailleur, J.; Bryant, G.; Pusey, P.; Poon, W. C. *Phys. Rev. Lett.* **2011,** 106, 018101.